Metallurgy and materials
Metalurgia e materiais

Effects of Te additions and stirring in the In segregation in $Ga_{1-x}In_xSb$ alloys

http://dx.doi.org/10.1590/0370-44672015690167

Cândida Cristina Klein
Professora Auxiliar
Universidade do Vale do Rio dos Sinos - UNISINOS
Doutoranda
Universidade Federal do Rio Grande do Sul – UFRGS
Departamento de Metalurgia
São Leopoldo - Rio Grande do Sul – Brasil
candidaklein@gmail.com

Berenice Anina Dedavid
Professora Titular
Pontifícia Universidade Católica do Rio Grande do Sul – PUCRS
Faculdade de Engenharia
Departamento de Engenharia Mecânica e Mecatrônica
Porto Alegre – Rio Grande do Sul – Brasil
berenice@pucrs.br

Kendra D' Abreu Neto Fernandes
Mestre em Engenharia em Tecnologia de Materiais
Pontifícia Universidade Católica do Rio Grande do Sul – PUCRS
Faculdade de Engenharia
Departamento de Engenharia Mecânica e Mecatrônica
Engenheira Química na empresa Satocao LDA
Morro do Peixe - Distrito de Lobata,
em São Tomé e Príncipe
kendraneto@hotmail.com

Nestor Cezar Heck
Professor Titular
Universidade Federal do Rio Grande do Sul - UFRGS
Escola de Engenharia
Departamento de Metalurgia
Porto Alegre – Rio Grande do Sul – Brasil
heck@ufrgs.br

Abstract

The influence of tellurium in the indium segregation of $Ga_{1-x}In_xSb$:Te ingots obtained by the conventional vertical Bridgman method (CVBM), under stirred and non-stirred conditions, was investigated. Three Te-doped ingots and three no-doped ingots were unidirectionally solidified at a constant speed of 2.0 mm/hour, inside quartz ampoules, closed under argon, and with a conical tip. The furnace temperature was set for overheating between 73.5 – 93°C, and temperature gradients between 3.0 – 3.3°C/mm. The tellurium doped ingots showed a smaller number of grains and no cracks in the middle region of the ingots, right after the tip, in comparison with the no-doped ingots. Moreover, when comparing the stirred with the non-stirred ingots, the EDS experimental profile of indium in Te-doped synthetized without melt stirring ingot showed a better agreement with the Scheil–Gulliver equation than the stirred Te-doped ingots. The Te-doped ingots when stirring the melt during synthesis showed a more constant axial indium distribution, up to 85% of their lengths. The constant lattice estimated from TEM diffraction images are respectively 6.29 Å for the non-doped sample and 6.17 Å for the Te-doped sample. A qualitative account for the increase of the lattice parameter and the Hall measurements results is that the tellurium compensates for the native acceptor defects, contributing to the microstructural quality in the $Ga_{1-x}In_xSb$ ingots.

Keywords: compound semiconductor III-V, bulk crystals, vertical Bridgman, GaInSb, tellurium.

1. Introduction

The $Ga_{1-x}In_xSb$ alloy is a very attractive III–V semiconductor for numerous substrate applications used in infrared (IR) and near IR devices (Dhanaraj *et al.*, 2010). The binary counterparts of GaSb and InSb are very miscible; both in the liquid and solid state. In this way the physical, electronic and optical properties of the $Ga_{1-x}In_xSb$ alloy may vary continuously with the InSb content in the alloy. The band gap and lattice constant of this alloy can be tuned from 0.70 to 0.18 eV and 6.1 to 6.5 Å, respectively (Dhanaraj *et al.*, 2010; Liu *et al.*, 2010).

Non-doped GaSb is invariably *p*-type in nature, due to the presence of native defects, such as gallium antisites (Ga_{Sb}) and $V_{Ga}Ga_{Sb}$ complex defects, which act as native acceptors (Shao *et al.*, 2007; Vlasov *et al.*, 2010). The non-doped InSb is *n*-type, due to the presence of V_{Sb} native defects, and the donor intrinsic concentration is roughly 10^{16} cm^{-3}, the same as for the acceptor concentration of GaSb (Adachi, 2009). The $Ga_{1-x}In_xSb$ alloys receive the native defects of the two compounds, proportionally. The transi-

tion from *p*-type to *n*-type occurs along the solidification axis at the ending part of $Ga_{1-x}In_xSb$ ingots, in the vertical Bridgman method (Adachi, 2009; Fernandes *et al.*, 2012; Dhanaraj *et al.*, 2010). The Bridgman vertical method is the most suitable unidirectional solidification process to obtain large-diameter $Ga_{1-x}In_xSb$ alloy ingots (Dutta, 2011).

Ternary ingot growth requires a small temperature gradient and a low growth rate (Kim *et al.*, 2006). However, it is well known that eliminating the segregation that causes the constitutional supercooling in ternary alloys during directional solidification, is not easy. The segregation that settles in front of the solid-liquid interface during the advance of solidification process produces ingots without uniform spatial composition and hence with no homogeneous electrical and optical properties (Dhanaraj *et al.*, 2010; Dutta, 2005, 2011; Goza *et al.*, 2011). Indium has a distribution coefficient $k_o<1$ in $Ga_{1-x}In_xSb$ (Dario *et al.*, 2011).

In the last years, several research groups have investigated the possibility of producing homogenous high-quality ternary bulk crystals of $Ga_{1-x}In_xSb$ using the conventional and non-conventional Bridgman method (Goza *et al.*, 2011; Dutta, 2011). Approaches such as solidification under microgravity, stirring, magnetic field in melt, and submerged baffle help avoiding dendritic structures in ingots, but with relative success (Dutta, 2011; Nobeoka *et al.*, 2014; Kozhemyakin *et al.*, 2014; Lyubimova *et al.*, 2014).

In this paper, we explore another possibility for decreasing the segregation of indium in GaInSb with the addition of tellurium as a dopant. The tellurium doping not only has the purpose of changing electrical parameters, but it is also effective in helping to decrease the native defects and dislocations, and is a factor that rules the crystalline quality and spatial composition in the GaSb and InSb ingots (Kaddeche *et al.*, 2015).

Tellurium atoms can take the place of Sb atoms, minimizing the Ga_{Sb}, $V_{Ga}Ga_{Sb}$ and V_{Sb} native defects of $Ga_{1-x}In_xSb$ alloys. Similarly, the tellurium atoms may bind to the interstitials gallium and indium in the solid during the solidification of $Ga_{1-x}In_xSb$, possibly decreasing the crystallographic defects (Shao *et al.*, 2007). Thus, the main purpose of this paper is to seek information on the tellurium behavior as a dopant in the indium distribution on $Ga_{1-x}In_xSb$ ingots obtained through the vertical Bridgman method.

2. Material and methods

Three non-doped and three tellurium doped with 10^{20} atoms.cm^{-3} $Ga_{1-x}In_xSb$ ingots with the molar composition of 10 % and 20% of InSb were produced. The alloys were prepared from the 6N pure pieces of GaSb and InSb in stoichiometric proportion, and 9N pure pieces of tellurium. For the synthesis and growth, the GaInSb alloys were melted inside quartz ampoules of 12 mm of diameter and 120-150 mm of length with a conical tip of 30° and the length <30 mm. The conical tip enables the elimination of some grains, favoring the single crystal growth.

The ampoules were previously etched with a solution of 50% HF + 50% distilled water for 2 hours, followed by rinsing with ethanol and water. After loading with alloy input materials, the ampoules were alternately filled with high-purity argon and evacuated (to 10^{-3} Torr) for over ten times. The ampoules were sealed under a small residual argon pressure.

The vertical Bridgman furnace used has a cylindrical oven chamber with 40 mm inside diameter and 240 mm length. The bottom-cooling chamber with 150 mm of length in the oven exit has the purpose of avoiding the thermal shock of the ingot material.

The method used in the alloy synthesis was to melt the materials for 12 h in the heating zone of the Bridgman furnace at 800 °C. During the synthesis, both C and D ingots (from B, C and D set) were stirred mechanically, every 15 minutes for 6 hours in order to improve the melting of the components. Finally, the ampoules passed through the solidification zone at a speed of 4.0 mm/hour.

For the growth, the furnace temperature was set to the lowest possible value to ensure a low thermal gradient during the solidification. Each ampoule remained 3 h in the heating zone of the furnace in order to ensure complete melting of the charge. Then it began to be vertically dislocated at a speed of 2 mm/h until it was completely out of the bottom-cooling chamber.

After an easy extraction from the quartz ampoule, the ingots were embedded in epoxy resin to avoid being mechanically damaged during the cut, lapping and polishing. The GaInSb ternary alloys are fragile and extreme care is necessary. One-half of each ingot was prepared for metallographic analysis in order to reveal the longitudinal indium compositional profile and crystallographic structure by Energy Dispersive Spectroscopy (EDS) with an Edax® Apollo X-SDD METEX detector coupled to a FEG Inspect F50 – FEI® and a SEM Philips XL30.

The other half was cut transversely into eight (0 to 7) parts. The transversal sections 0, 2, 4 and 6 were used for electrical conductivity and Hall measurements. The 5 x 5 x 2 mm lapped and polished transversal samples were measured with the ECOPIA HMS-3000 system under a 0.55 T magnetic field at room temperature. In order to obtain the ohmic contacts, the eutectic gallium-indium dots were used. The Van der Pauw method was used to determine the carrier concentration (*n*), carrier mobility (μ), and resistivity (ρ).

Transversal sections #3 of the B1 and B2 ingots showed good structural quality; therefore, they were chosen for the transmission electron microscope (TEM) observation. These transversal samples were characterized with the JEOL JEM/STEM-2010 and a FEI-Tecnai 2G-Xtwin STEM, both operating at 200 kV. Thin TEM specimens were prepared by conventional methods, including cutting, grinding, dimpling, polishing and low-energy Ar-ion milling equipped with a liquid nitrogen cooling stage.

3. Results

Solidification microstructures of the tip, middle and top longitudinal regions for the $Ga_{0.9}In_{0.1}Sb$ ingot (D1), $Ga_{0.9}In_{0.1}Sb$:Te ingot (D2) and $Ga_{0.8}In_{0.2}Sb$:Te ingot (C2) are shown in Figure 1. Notice the crack presence in the Te-doped and non-doped ingots. However, the ingots D1 and D2, with In 10% molar, show large monocrystalline areas in the middle regions, while the C2 ingot, with more In content (20% molar), shows small grains in the middle

region, as respectively exemplified by the Figures 1 (c), (d), and (b). Some of the tip cracks in Figure 1 do not have the origin in crystallographic stress but are due to the handling and cutting of the samples.

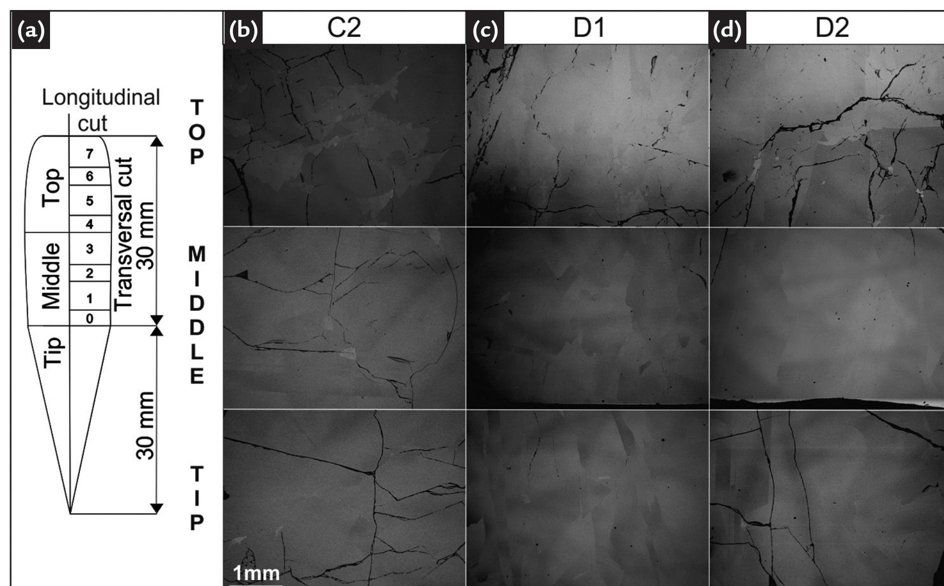

Figure 1
a) Samples taken from ingots: longitudinal (tip, middle and top) and transversal parts (0 to 7). SEM/BSE image of the tip, middle and top regions of the longitudinal samples of C2 (b), D1(c) and D2 (d) ingots. The lighter regions denote a greater presence of indium and the darker, of gallium. The black lines in images (b), (c) and (d) are cracks.

In the vertical Bridgman method, the Scheil–Gulliver model $C_s=kC_o(1\text{-}g)^{(k\text{-}1)}$ represents the segregation profile assuming complete diffusion in the liquid and no diffusion in the solid (Dario *et al*., 2011). Hence, at a given temperature with local equilibrium between the phases, the incorporation of impurity atoms during a phase transformation is characterized by the equilibrium segregation coefficient *k* (Duhanian *et al*., 2005). This coefficient is defined as the ratio between the solute concentration in the solid (C_S) and in the liquid (C_L) at the solid/liquid interface. However, true equilibrium never exists for a crystallization process where the interface advances with a finite rate. Therefore, in this case the effective segregation or distribution coefficient, k_{eff}, must be used.

The k_{eff} describes the overall incorporation of solute into the solid, in a near-equilibrium solidification state, when the interface advances with a finite velocity (Burton *et al*., 1953). Table 1 shows the composition, the thermal conditions during the synthesis and growth, along with the indium effective segregation coefficient k_{eff} for all of the six ingots from this experiment. The k_{eff} was determined using the Scheil–Gulliver equation, with data from the EDS compositional analyses.

Table 1
Initial alloys, overheating condition, and axial thermal gradient between *liquidus* and *solidus* temperature.

Ingot	Alloys	Overheating condition (°C)		Thermal Gradient (°C/mm)	k_{eff} indium (R^2)
		Synthesis	Growth		
B1	$Ga_{0.8}In_{0.2}Sb$	105.5	73.5	3.0	0.21 (0.8372)
B2	$Ga_{0.8}In_{0.2}Sb$:Te	105.5	73.5	3.0	0.22 (0.8253)
C1*	$Ga_{0.8}In_{0.2}Sb$	105.5	73.5	3.0	0.21 (0.8497)
C2*	$Ga_{0.8}In_{0.2}Sb$:Te	105.5	73.5	3.0	0.24 (0.8561)
D1*	$Ga_{0.9}In_{0.1}Sb$	93	93	3.3	0.21 (0.9036)
D2*	$Ga_{0.9}In_{0.1}Sb$:Te	93	93	3.3	0.23 (0.8081)

(*) Ingots with melt stirring during the synthesis. Indium effective segregation coefficient k_{eff}(in brackets the coefficient of determination R^2).

Figures 2 (a) , (b), (c), and (d) show the compositionally normalized indium profiles (C_s/C_o) of the B1, B2, C1 and C2 ingots, respectively. The tellurium was not considered to be outside the detection limit of the EDS microanalysis. The full line in the Figures 2 (a), (b), (c), and (d) represent the Scheil–Gulliver equation obtained with the experimental effective segregation coefficient shown in Table 1.

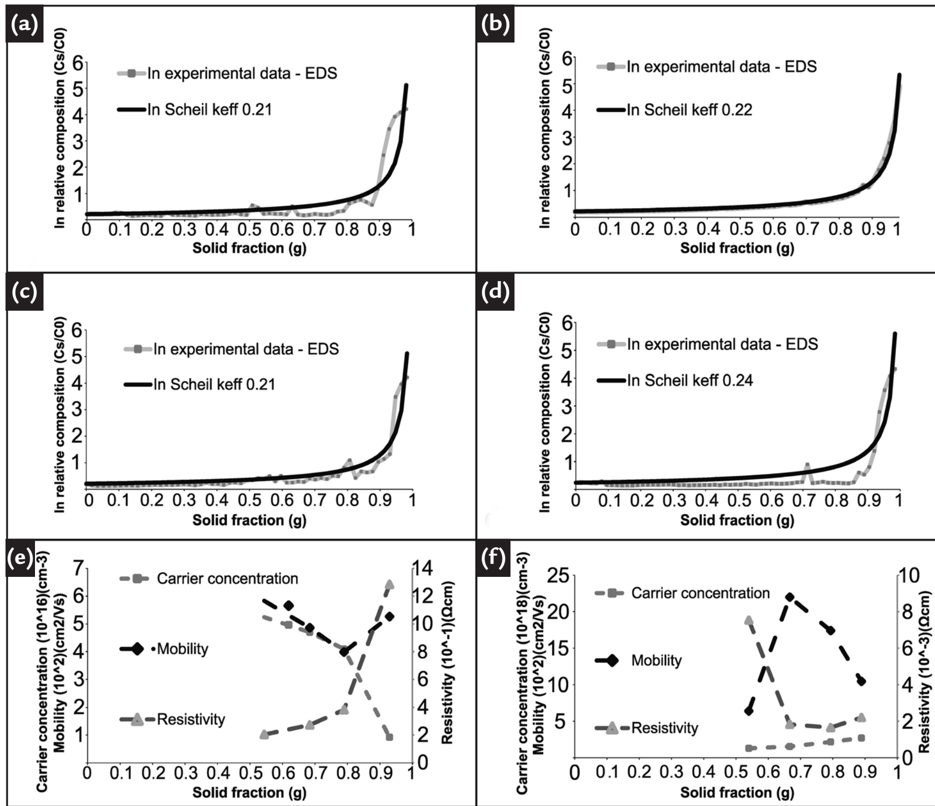

Figure 2
Graphs (a), (b), (c) and (d) show the composition variation along of ingot B1, B2, C1 and C2, respectively, measured in the central axis of the ingots by EDS. Graphs (e) and (f) show the electrical properties of the transversal sections 0, 2, 4 and 6 for the B1 and B2 ingots.

Figures 2 (a), (c) and (d) show that there are differences between the experimental indium profiles of the B1, C1 and C2 ingots and the Scheil–Gulliver equation. Notice that the indium profile of the B2 ingot (non-stirred, Te-doped) is what best fits the Scheil–Gulliver equation when compared to the B1 ingot (non-stirred, non-doped) and the others melt stirred in the synthesis. Note that the indium profile is very similar for non-doped ingots B1 and C1 when compared with Te-doped ingots B2 and C2. The C2 ingot shows the indium profile unchanged up to 85% of length. Following, Figures 2 (e) and 2 (f) show the electric characteristic by Hall measurement in transversal sections 0, 2, 4 and 6, for the B1 and B2 ingots.

Observe that in the graphs of Figures 2 (e) and (f), the Te-doped ingot (B2) shows around 10^2 times lower resistivity, 10^2 times higher carrier concentration than the non-doped ingot (B1). Notice that mobility remains almost unchanged. All of the Te-doped ingot transversal samples show *n*-type conductivity, indicative of the tellurium activity as dopant. In contrast, transversal sections 0, 2, 4 and 6 of non-doped ingots melt stirred in the synthesis show *p*-type conductivity. The transversal section 6 of the B1 ingot, non-stirred in the synthesis shows *n*-type conductivity. The behavior of B1 ingot is referred to the ratio Ga/In < 1 in cross section 6.

The HRTEM images and diffraction patterns from #3 transversal sections of B1 and B2 ingots, in the monocrystalline regions grown in [101] and [112] directions respectively are shown in Figure 3.

The TEM analyses of the B1 and B2 ingots transversal samples show the presence of dislocations. However, the dislocations observed in the B1 ($Ga_{0.8}In_{0.2}Sb$) transversal sample ingot are clusters (Figure 3 (a)) and in the B2 ($Ga_{0.8}In_{0.2}Sb$:Te) ingot, they are in line (Figure 3 (e)).

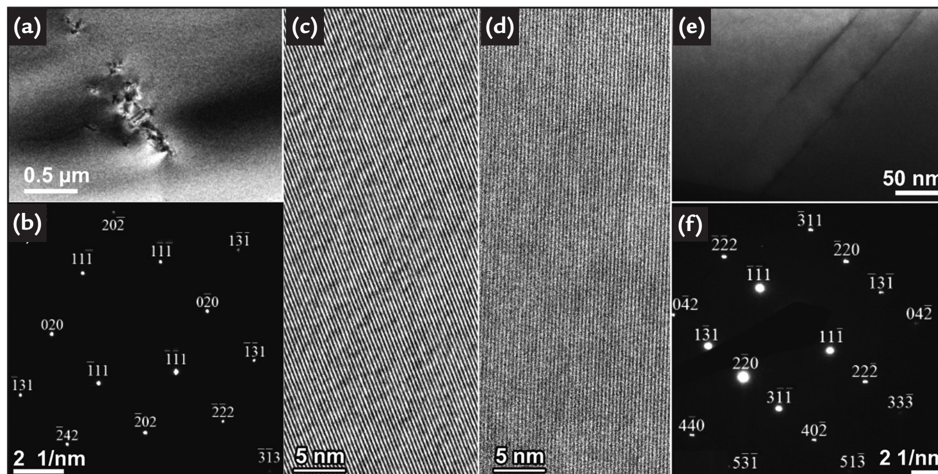

Figure 3
TEM Bright-field (BF) images of #3 transversal sections taken from B1 ($Ga_{0.8}In_{0.2}Sb$) and B2 ($Ga_{0.8}In_{0.2}Sb$:Te) ingots. Images (a) and (e) show dislocations decorations; (b) and (f) diffraction patterns, and (c) and (d) HRSTEM images of B1 and B2 ingots.

Notice that, the doped ingot matrix appears more homogeneous in Figure 3 (d) than the non-doped ingot matrix (Figure 3 (c)).

4. Discussion

The experimental results show large monocrystalline areas in the middle regions, right after the tip region for D1(non-doped, stirred, In 10% molar) and D2 (Te-doped, stirred, In 10% molar) ingots, as Figure 1 exemplifies. The C2 (Te-doped, stirred, In 20% molar) ingot shows small grains in the middle region but in less quantity than in the tip and in the top. This behavior can be understood in two ways, i.e., as a brief solid-liquid interface stabilization, consequence of the tip edge, or as an effect of the constitutional supercooling. In the first case, the edge angle drives the grain growth toward the central axis of the ampoule, in the opposite direction of the thermal gradient established (Nobeoka *et al*., 2014). The grain competition results in a loss of some of them, promoting the stabilization of the interface (Reijnen *et al.,* 2005).

In the other case, considering the experimental report of Dutta (2005, 2011), it can be assumed that large monocrystalline areas in mid-regions, in D1 and D2 ingots, are due to the smaller molar composition of indium (10%) when compared to the indium molar composition of the C2 ingot (20%). The grains in the mid-region of the C2 ingot indicate the effect of the constitutional supercooling that promotes the interface breakdown when indium content fluctuates, as shown in Figure 1(b). The indium has k_{eff}<1, thus it segregates to the liquid. Although Te and In are different entities for the GaSb system (Kim *et al*., 2006), these considerations suggest that differences in microstructure observed between C2 and D2 may be mainly attributed to the distinct indium concentration.

Thus, in the top of the ingots, when the constitutional supercooling is well established, due to a larger amount of segregated indium, the interface is destabilized and consequently, dendritic grains are grown (Reijnen *et al*., 2005; Gadkari, 2013).

Moreover, the lower crack density observed in the middle regions of the ingots when compared to the ingot tops (Figure 1) should also be attributed to the low concentration of indium segregated in these regions, since the solidification rate used for this study (2.0 mm/h) is almost 10 times greater than the recommended by Dutta (2005) to crack elimination. Nevertheless, the crack density found in the ingots is lower than the figures reported in literature (Vincent and Diéguez, 2006; Dutta, 2011).

Although the k_{eff} segregation coefficient shows little difference between the ingots, and the thermal conditions in the synthesis and growth were the same (Table 1), the indium profile are different when compared to the Scheil–Gulliver equation (Figure 2). These differences are more pronounced between the indium profile of B2 (Te-doped, non-stirred, In 20% molar) ingot and the C2 (Te-doped, stirred, In 20% molar) ingot. This can be a consequence of melt stirring during the synthesis (Lyubimova, *et al*., 2014; Kim *et al.,* 2006). The mechanical stirring during the ingots synthesis mixes the remaining melt in front of the solid-liquid interface, making the indium dispersion more homogenous. Thus, the non-stirred ingots show an indium profile related to two consecutive unidirectional solidifications (Kim *et al*., 2006). On the other hand, the stirred ingots show an indium compositional profile correlated with a single directional solidification process, starting from more homogeneous indium profile ingots. The fact that the stirred ingots show a better longitudinal distribution of the indium than non-stirred ingots was also reported by Kim *et al*. (2006). Furthermore, the fact that B1 is the single ingot with changing conductivity from *p* to *n* type in transversal sample 6 can also be considered as a consequence of not having been stirred during synthesis. Samples stirred in the synthesis C1 and D1 are *p*-type for all transversal sections 0, 2, 4 and 6.

The existence of more extensive and better-defined monocrystalline areas in the doped ingots (Figure 1) can be a consequence of tellurium in the lattices of the GaInSb. To be specific, it is known that the tellurium doping benefits the microstructural quality of the GaSb crystals grown by the Bridgman method (Vlasov *et al.,* 2010). The literature reports also that the decrease in dislocation density in Te-doping GaSb and InSb ingots is attributed to lattice hardening (Vlasov *et al*., 2010). The lattice constant of $Ga_{0.8}In_{0.2}Sb$ is 6.16 Å, according to the Vegard equation (Dutta, 2011). For #3 transversal sections of B1 and B2 ingots, the lattice constant estimate from the diffraction images (Figure 3 (b) and 3 (f)) are respectively 6.29 Å for non-doped transversal sample and 6.17 Å for Te-doped transversal sample. The smallest difference between the lattice parameter found by Dutta (2011) and in the sample of B2 Te-doped can be attributed to Te_{Sb} defect. The tellurium atomic radius (0,140 nm) is similar to antimony atomic radius (0,145 nm); therefore, the Te_{Sb} defect should not drastically alter the lattice spatial equilibrium and does not generate a large tension on the crystal lattice, but can cause the decrease of V_{Sb} vacancies, Ga_{Sb}, $V_{Ga}Ga_{Sb}$, or other native defects of GaInSb.

In general, the Te-doping may cancel or produce native defects, in order to change the conductivity of the GaInSb alloys from *p*-type to *n*-type, as the Hall measurement shows. The increase of donor concentration and the conductivity to 10^2 times, with little variation of mobility, in the Te-doping ingots (Figure 2 (e) and 2 (f)) is very interesting, and can be understood with a V_{Sb} native defects compensation. The native defects In_{Sb}, Ga_{Sb} and V_{Sb} are considered *p*-type and tellurium substitutional defect (Te_{Sb}) is *n*-type, in GaInSb lattice (Pino *et al*., 2004). Therefore, Te_{Sb} defect should compensate those acceptor defects, contributing to lattice hardening and better crystallographic organization and indium distribution, as shown in Figure 2 (b) and (d).

5. Conclusion

In summary, the present study shows that tellurium doping is reproducible, ensures the enhancement of the indium segregation and microstructural quality on $Ga_{1-x}In_xSb$ ingots. Tellurium doping has an impact on the crack formation of $Ga_{1-x}In_xSb$ ingots to x=0.1 and 0.2 mole fractions. In the vertical Bridgman method, the indium segregation for the $Ga_{1-x}In_xSb$:Te ingot non-stirred during synthesis shows a better fit to the Scheil–Gulliver model than the no-stirred and non-doped condition. The Te-doped ingots melt stirred during synthesis show a constant axial indium distribution up to 85% of their lengths. A qualitative account for the increase of lattice parameter and result of the Hall measurements is that the tellurium atoms is a substitutional defect (Te_{Sb}) that should compensate for the acceptor native defects, contributing

to lattice hardening, to decrease the microstructural defects and, therefore to a more constant indium distribution in 85% of the GaInSb:Te ingot length.

6. Acknowledgment

The authors would like acknowledge the financial support from the CNPq/ CAPES CHAMADA PÚBLICA Nº 06/2011 – CASADINHO/PROCAD - n. 552415/2011-1

7. References

ADACHI, S. ***Properties of semiconductor alloys: group-IV, III–V and II–VI semiconductors.*** London: John Wiley & Sons, 2009. 422p.

BURTON, J. A., PRIM, R. C., SLICHTER, W. P. The distribution of solute in crystals grown from melt. Part I. Theoretical. ***The Journal of Chemical Physics,*** v. 21, p. 1987-1991, 1953.

DARIO, A., SICIM, O.H., BALIKCI, E. A new approach for dopant distribution and morphological stability in crystals grown by the axial heat processing (AHP) technique. ***Journal of Crystal Growth***, v. 337, p. 65–71, 2011.

DHANARAJ, G., BYRAPPA, K., PRASAD, V., DUDLEY, M. ***Springer Handbook of Crystal Growth.*** Berlin; London: Springer, 2010. 1816p.

DUHANIAN, N., DUFFAR, T., MARIN, C., DIEGUEZ, E, GARANDET, J. P., DANTAN, P., GUIFFANT, G. Experimental study of the solid–liquid interface dynamics and chemical segregation in concentrated semiconductor alloy Bridgman growth. ***Journal of Crystal Growth,*** v. 275, p. 422–432, 2005.

DUTTA, P. S. Bulk growth of crystals of III – V compound semiconductor. In: BHATTACHARYA P., FORNARI R, and KAMIMURA, H. (eds.). ***Comprehensive Semiconductor Science and Technology.*** Amsterdam: Elsevier, n.3, p. 36 – 80, 2011.

DUTTA, P. S. III–V Ternary bulk substrate growth technology: a review. ***Journal of Crystal Growth,*** v. 275, p. 106-112, 2005.

FERNANDES, K. N. D., DEDAVID, B. A., STREICHER, M. Comportamento segregacional do índio em cristais $Ga_{1-x}In_xSb$ obtidos pelo método Bridgman vertical. In: CONGRESSO BRASILEIRO DE ENGENHARIA E CIÊNCIA DOS MATERIAIS, 20, 2012. Joinville. Anais eletrônicos, 2012. Disponível em: <http://www.cbecimat.com.br/trabalhos-completos-cbecimat.php>

GADKARI, D. Detached phenomenon: Its effect on the crystal quality of $Ga_{(1-x)}In_xSb$ bulk crystal grown by the VDS technique. ***Materials Chemistry and Physics***, v. 139, p. 375–382, 2013.

GOZA, A. J., TRITCHLER, S. E., BLISS, D. F., HOUCHENS, B. C. Thermodynamic modeling of bulk ternary alloy crystal growth: Comparison of experiments and theory for GaInSb alloys. ***Journal of Crystal Growth,*** v. 337, p. 60–64, 2011.

KADDECHE, M., GARANDET, J. P., HENRY, D., HADID, D. H., MOJTABI, A. On the effect of natural convection on solute segregation in the horizontal Bridgman configuration: Convergence of a theoretical model with numerical and experimental data. ***Journal of Crystal Growth,*** v. 409, p. 89–94, 2015.

KIM, H. J., CHANDOLA, A., BHAT, R.; DUTTA, P.S. Forced convection induced thermal fluctuations at the solid–liquid interface and its effect on the radial alloy distribution in vertical Bridgman grown $Ga_{1-x}In_xSb$ bulk crystals. ***Journal of Crystal Growth,*** v. 289, p. 450–457, 2006.

KOZHEMYAKIN,G.N., NEMETS, L.V., BULANKINA, A.A. Simulation of ultrasound influence on melt convection for the growth of $Ga_xIn_{1-x}Sb$ and Si single crystals by the Czochralski method. ***Ultrasonics,*** v. 54, p. 2165–2168, 2014.

LIU, C., LI, Y., ZENG, Y. Progress in Antimonide Based III-V Compound Semiconductors and Devices. ***Engineering,*** v. 2, p. 617 – 624, 2010.

LYUBIMOVA, T. P., LYUBIMOV, D. V., IVANTSOV, A. O. The influence of vibrations on melt flows during detached Bridgman crystal growth. ***Journal of Crystal Growth,*** v. 385, p. 77–81, 2014.

NOBEOKA, M., TAKAGI, Y., OKANO, Y., HAYAKAWA, Y., DOST, S. Numerical simulation of InGaSb crystal growth by temperature gradient method under normal- and micro-gravity fields. ***Journal of Crystal Growth,*** v. 385, p. 66–71, 2014.

PINO, R., KO, Y., DUTTA, P.S. High-resistivity GaSb bulk crystals grown by the vertical Bridgman method, ***Journal of Electronic Materials***, v. 33, n. 9, 2004.

REIJNEN, L., BRUNTON, R., GRANT, I.R. GaSb single-crystal growth by vertical gradient freeze. ***Journal of Crystal Growth,*** v. 275, p. e595–e600, 2005.

SHAO, Y.D., WANG, Z., DAI, Y.Q., ZHAO, Y.W., TANG, F.Y. Identification of vacancies in electron irradiated GaSb by coincidence Doppler broadening spectroscopy. ***Materials Letters,*** v. 61, p. 1187 – 1189, 2007.

VINCENT, J., DIÉGUEZ, E. Microstructure and solidification behavior of cast GaInSb alloys. ***Journal of Crystal Growth,*** v. 295, p. 108–113, 2006.

VLASOV, A.S., RAKOVA, E.P., KHVOSTIKOV, V.P., SOROKINA, S.V., KALINOVSKY, V.S.; SHVARTS, M.Z.; ANDREEV, V.M. Native defect concentration in Czochralski-grown Te-doped GaSb by photoluminescence. ***Solar Energy Materials & Solar Cells,*** v. 94, p. 1113 – 1117, 2010.

Received: 23 October 2015 - Accepted: 21 June 2016.